



1 Article

2 Saccharomyces cerevisiae and Candida albicans yeast

cells labeled with Fe(III) complexes as MRI probes

- 4 Akanksha Patel,¹ Didar Asik,¹ Eric M. Snyder,¹ Joseph A. Spernyak,³ Paul J. Cullen² and Janet R.
- 5 Morrow^{1,*}
- Department of Chemistry, University at Buffalo, The State University of New York, Amherst, NY 14260, USA; aparetel27@buffalo.edu (A. P.); didarasi@buffalo.edu (D. A.); ericsnyd@buffalo.edu (E. M. S.)
- Department of Biology, University at Buffalo, The State University of New York, Amherst, NY 14260, USA;
 pjcullen@buffalo.edu (P. J. C.)
- Department of Cell Stress Biology, Roswell Park Comprehensive Cancer Center, NY 14263, USA; joseph.spernyak@roswellpark.org (J. A. S.)
- * Correspondence: <u>imorrow@buffalo.edu</u>
- Received: date; Accepted: date; Published: date

14 Abstract:

The development of MRI probes is of interest for labeling antibiotic-resistant fungal infections based on yeast. Our work shows that yeast cells can be labeled with high spin Fe(III) complexes to produced enhanced T₂ water proton relaxation. These Fe(III) based macrocyclic complexes contain a 1,4,7-triazacyclononane framework, two pendent alcohol groups and either a non-coordinating ancillary group and a bound water or a third coordinating pendant. The Fe(III) complexes that have an open coordination site associate strongly with *Saccharomyces cerevisiae* upon incubation as shown by screening using Z-spectra analysis. Incubation of one Fe(III) complex with either *Saccharomyces cerevisiae* or *Candida albicans* yeast leads to interaction with the β-glucan based cell wall as shown by the ready retrieval of the complex by the bidentate chelator, Maltol. Other conditions such as heat shock treatment of the complexes produces Fe(III) complex uptake that cannot be reversed by addition of Maltol. Appending a fluorescence dye to Fe(TOB) leads to uptake through secretory pathways as shown by confocal fluorescence microscopy and by the incomplete retrieval of Fe(III) complex by Maltol treatment. Yeast cells that are labeled with these Fe(III) complexes display enhanced water proton T₂ relaxation, both for *S. Cerevisiae* and for yeast and hyphal forms of *C. albicans*.

Keywords: Fe(III) complexes; cell labeling; T2 contrast; invasive candidiasis; MRI

1. Introduction

There are many applications that involve the use of chemical probes for tracking various types of cells. For example, tracking of mammalian cells is important for cell therapy approaches whereas the monitoring of microbes may be useful for studying infections. Cell therapy is an emerging method in regenerative medicine with applications in cancer therapy, treating genetic disorders and enabling repair of damaged cells.[1-3] In certain cell therapy applications, the cells are modified *ex vivo* and later implanted into the body. Imaging these cells *in vivo* would provide real-time distribution and assessment of the therapeutic cells. One imaging modality, MRI, has the advantages of unlimited depth penetration, high spatial resolution and the use of non-ionizing radiation. Mammalian cells labeled with paramagnetic MRI contrast agents have been employed in preclinical studies.[2,4-6] The cell labeling approach may be extended to image bacterial and fungal pathogens, to investigate onset and progression of infectious diseases. To date, there are several

reports of PET (positron imaging tomography) probes for *in vivo* imaging of bacteria or fluorescent agents.[7,8] However, chemical probes that facilitate the MR imaging of microbial infections such as fungal infections are underdeveloped.

Over 90% of fungal infections are caused by commensal candida species, termed as candidiasis, which are a major cause of mortality in immunocompromised patients despite the availability of antifungal treatments.[9-14] Candidiasis is caused by several fungal species, including *Candida albicans*, which typically resides on the mucocutaneous surfaces of the human body. It is a polymorphous fungus as shown by its ability to undergo morphogenic changes (yeast, pseudohypha and hypha) triggered by environmental factors.[10,14-16] There is a strong correlation between the yeast to hyphal state transformation and pathogenicity of *C. albicans*.[9,11,17,18] The commensal nature of *C. albicans* and the seriousness of the infections caused by these organisms calls for better diagnostic procedures and more sophisticated disease models as well as tools for studying infections.

Despite the impressive soft tissue contrast in MRI, the images of yeast are dependent on the structural abnormalities caused by the infection.[19,20] Often, immunocompromised patients with widespread infections are the subject of these studies.[19,21,22] There is critical need for a non-invasive and accurate diagnostic test for fungal infections. Furthermore, tools for tracking yeast *in vivo* through imaging to study infections in animal models would be useful for monitoring therapeutic treatments.[23]

Scheme 1. Fe(III) complexes shown with predominant species at neutral pH

Our group has developed a new class of high spin Fe(III) complexes that are effective MRI contrast agents. [24-26] These robust complexes display promising T_1 MRI contrast both *in vivo* and in vitro experiments. All complexes contain a triazacyclononane (TACN) framework with two or three coordinating hydroxypropyl pendants to bind the small Fe(III) metal ion and stabilize the trivalent oxidation state (Scheme 1). The hydroxypropyl groups provide strong interactions with second sphere water to increase relaxivity. Four of the complexes studied here (Fe(TOBA), Fe(TOD) and Fe(TASO)) have a water as a sixth ligand in order to increase water proton relaxivity. Notably, this open coordination site is important in producing complexes that bind to small molecules such as bidentate chelates as well as macromolecules such as polymeric β -glucan particles. [27] Two of the complexes, Fe(TOT), and Fe(TOTz) are coordinatively saturated and lack an innersphere water to give complexes with limited interactions with biopolymers or other ligands. All complexes have a single deprotonated hydroxypropyl pendant and an overall cationic charge.

In this study, we screened five high spin Fe(III) complexes shown in Scheme 1 and studied the feasibility of labeling *Saccharomyces cerevisiae* (Baker's yeast), a model organism with properties

related across many species including pathogens. The most promising derivatives were also studied on pathogenic Candida albicans. Cell association was optimized in S. cerevisiae using heat shock and endocytosis. Endocytosis was found to be the most efficient mode of cell treatment and was used to label C. albicans with Fe(TOB). Fe(TOD), a fluorescent analogue of Fe(TOB) enabled us to investigate the localization of these complexes in cells.[27] A previous study in our group showed yeast cells with an Fe(III) complex containing a coumarin dye, but the complex was not sufficiently soluble for loading cells with high concentrations of paramagnetic complex.[26] The nature of the cellular association and localization of Fe(TOB) or Fe(TOD) labeling of cells was further probed by using a small molecule chelator maltol which we have shown to sequester Fe(III) complexes from glucan particles derived from yeast by formation of a ternary adduct.[27] We show here that both S. cerevisiae and C. albicans displayed enhanced R2 relaxation properties when labeled with the Fe(TOB) complex.

2. Results

2.1. Yeast cell culture

Experiments with Fe(III) coordination complexes were conducted on *S. cerevisiae* and subsequently extended to *C. albicans*. Yeast cells used in the study are *S. cerevisiae of the Sigma1278b* strain background. [28] The specific strain used (PC538) is a typical wild-type (WT) strain with the following genotype: *MATa* ste4 FUS1-HIS3 FUS1-lacZ ura3-52, [29] which was used for all experiments in the study. The samples were normalized with respect to total protein content (biomass) in order to compare cell labeling across the strains. [30] A linear relationship between optical density of cultures and total protein content was obtained (Figure S12-S14). Samples were prepared by adjusting the optical densities to normalize the protein content for the experiments.

2.2. Labeling yeast cells

Endocytosis and heat shock incubation were employed to study the cellular association of Fe(TOB) in *S. cerevisiae*.[31] Both techniques exhibited promising iron complex cell association as analyzed by ICP-MS. Endocytosis was chosen as the preferred method since it induces less stress in the cells. Briefly, the cells were grown to mid log phase, harvested through centrifugation and washed with 1x PBS before Fe(III) complex treatment. The cells were incubated with the complex in 1x PBS for 30 min, and post incubation the cells were collected and washed with 1x PBS buffer. *C. albicans* were treated with Fe(TOB) using the optimized endocytosis protocol in *S. cerevisiae*. The resulting cell pellet was yellow-orange in color due to Fe(TOB) loading (Figure S1). All subsequent studies with Fe(III) complexes used endocytosis for labeling. Endocytosis was used for labeling of *S. cerevisiae* with Fe(TASO), Fe(TOBA), Fe(TOT) or Fe(TOTz). These complexes were chosen based on their effective r₁ and r₂ relaxivity, which is highest for the Fe(TOB), Fe(TOBA) and Fe(TASO) complexes that have an inner-sphere water (Table S1). Notably, r₂ values for Fe(TOB) and Fe(TOBA) are similar to those of Gd(DTPA) at 4.7 Tesla and 37 °C within experimental error. The r₁ value of Fe(TOB) is approximately 70% of Gd(DTPA) under these conditions.[25]

2.3. Z-spectra measurements

The *S. cerevisiae* samples were incubated with Fe(III) complexes and the Z spectra were recorded as an initial screen of labeling. Following harvesting and rinsing, the cells were suspended in 1x PBS and transferred to NMR tubes for Z-spectra measurements at irradiation power B_1 =3, 6, 12 μ T. Z-spectra are plots of the magnetization intensity of the bulk water signal upon irradiation with a presaturation radiofrequency pulse typically from 40 ppm to -40 ppm at 0.5 ppm intervals. The data are expressed as the percent reduction in the water proton magnetization (M_z/M_o). Z-spectra arise from contributions from T_2 effects as well as magnetization transfer effects, and may display asymmetry from chemical exchange saturation transfer (CEST) effects. At the outset of these studies, we hypothesized that the Fe(III) complexes would shift the water proton pool of the yeast cells to give rise to a CEST effect as we have observed in Fe(III) containing shrunken liposomes.[32]

Lanthanide containing liposomes show both CEST and broadening of the Z-spectra from T₂ –based magnetic susceptibility effects of paramagnetic complexes encapsulated in non-spherical compartments.[33]

--- FeTOB B₁ =3uT FeTOB B₁ =6uT M_z/M_o% FeTOB B₁ =12uT control B₁ = 3 uT control B₁ = 6 uT control $B_1 = 12 uT$ -10 -20 Chemical shift

Figure 1. Z-spectra of (a) control and (b) 10 mM Fe(TOB) labeled through endocytosis in *S. cerevisiae* in 1x PBS at 37 °C.

The *S. cerevisiae* samples labeled through endocytosis showed broadening of the Z-spectra (Figure 1, S4-S5) for the complexes that had an open coordination site including Fe(TOB), Fe(TOBA) and Fe(TASO). The broadening was most pronounced for heat shock treatment with Fe(TOB) (Figure S3). No apparent broadening of Z-spectra was observed when *S. cerevisiae* were treated with Fe(TOT) or Fe(TOTz) using similar incubation protocols (Figures S6-S7). We suspected that an interaction between Fe(TOB), Fe(TOBA) or Fe(TASO) and β -D-glucan present in cell wall of *S. cerevisiae* was responsible for the increased broadening of the Z-spectra. Supporting this postulate is a report showing that Fe(TOB) interacts with glucan particles derived from yeast cells, but Fe(TOT) has a much weaker interaction.[27] Further studies focused on Fe(TOB) or the fluorescent analog, Fe(TOD), for labeling of yeast.

Both *C. albicans* budding yeast and hyphae phenotypes were labeled with Fe(TOB) through endocytosis. The yeast phenotype exhibited similar broadening in the Z-spectra as observed in *S. cerevisiae* yeast (Figure S8). *C. albicans* hyphae on the other hand displayed enhanced broadening in the Z-spectra (Figure S9). The filamentous shape of the hyphae is likely to enhance the magnetic susceptibility resulting in greater T₂ effects as discussed below.

2.4. Fluorescence microscopy on S. cerevisiae

S. cerevisiae cells were treated with Fe(TOD) to investigate the localization of iron complexes in endocytosis. The photophysical properties of Fe(TOD) are reported in the literature.[27] *S. cerevisiae* cells were treated with 10 mM Fe(TOD) and incubated for 30 min at 30 °C. The cells were harvested and imaged with confocal fluorescence microscopy (Figure 2). The Fe(TOD) complex exhibited organeller compartmentalization that was most likely due to the complex being inside a vacuole.[31] No apparent fluorescence was observed in control cells under the same imaging conditions.

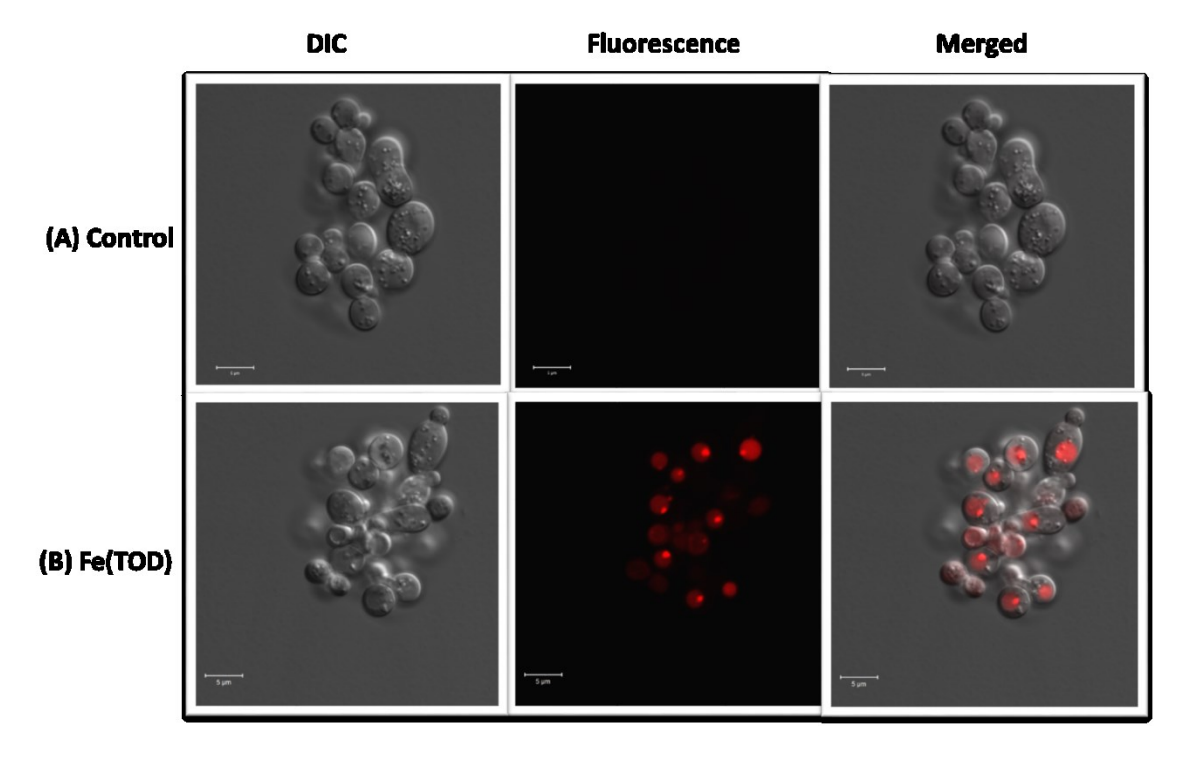


Figure 2. Confocal fluorescence microscopy images of *S. cerevisiae* PC538 cells. A) control cells (B) Fe(TOD) (10 mM) treated cells. DIC stands for differential interference contrast. Excitation (405 nm) emission (520-560 nm).

2.5. Sequestration of Fe(III) complexes from yeast with bidentate chelator.

Certain bidentate chelates, such as maltol, bind strongly to Fe(TOB) or Fe(TOD) to produce a ternary complex in which the macrocyclic ligand is retained.[27] Treatment with maltol can be used as a tool to study the release of Fe(TOB) or Fe(TOD) from labeled glucan particles.[27] Along similar lines, maltol treatment of Fe(TOB) labeled *S. cerevisiae* and *C. albicans* was monitored through NMR spectroscopy, ICP-MS and cell viability experiments. The Fe(TOB) labeled cells were treated with 10 mM Maltol solution and incubated at 30 °C for 3 h. The cell media turned red in color after maltol treatment, indicating the formation of the Fe(TOB)-Maltol ternary complex. The cells were washed and normalized with respect to the total protein content for the experiments.

2.6. Determination of Fe content in the yeast.

The cellular association of Fe(III) complexes was determined by using ICP-MS measurements of total iron content in the cells (Figure 3 and Figure S11). The Fe content was normalized with respect to total protein content for the purpose of comparison of different *S. cerevisiae* and *C. albicans* phenotypes.[34] The Fe(III) complex labeled cells displayed significantly higher iron content compared to control cells in both *S. cerevisiae* and *C. albicans*.

Among the various cell labeling methods studied on *S. cerevisiae*, endocytosis displayed significantly higher Fe(TOB) cell association than heat shock. This was surprising given the large broadening observed in the Z-spectra for heat shock labeled samples, which suggests cellular localization is important (Figure 3(a)). In comparison, Fe(TOT) displayed only 25% of the cellular association in live yeast cells that was observed with Fe(TOB). The lowered amount of Fe(TOT) in yeast was comparable to the lower loading observed in β –glucan based cell wall particles.[27] This observation suggests the labeling of the yeast cells with Fe(III) complexes is dependent on both charge and coordination sphere of the treated complexes. *S. cervisiae* labeled Fe(TASO), and Fe(TOBA)

184 185

197 198

199

200

showed iron levels that were roughly comparable to those of Fe(TOB), whereas Fe(TOTz) labeled cells were at 25% of those observed for Fe(TOB).

Maltol treatment of the control samples did not show any significant change in iron content, suggesting that Maltol cannot sequester iron from endogenous proteins or native iron pools. Maltol treatment of Fe(TOB) treated cells restored the iron content to the pre-Fe(TOB) treatment levels in endocytosis (Figure 3(a)). However, Maltol treatment of Fe(TOB) heat shocked cells did not restore the iron content of the cells to the pre-Fe(TOB) treatment levels. This result further substantiates a secretory pathway localization of complex during heat shock treatment.

Maltol treatment of cells labeled with Fe(TOD) through endocytosis did not decrease the iron levels to those of control (Figure 2(a)). Given that confocal fluorescence microscopy suggests organellar localization of Fe(TOD), the Fe(TOD)-Maltol complex would need to cross organellar membrane followed by cell membrane as well as cell wall to sequester the complex out of the cells. This process may be slow so that it was not complete after 3 h, or may not be feasible in the cells. Maltol treatment of cells labeled with Fe(TOT) did not reduce iron levels to that of control. This result is consistent with the fact that Fe(TOT) cannot form the ternary complex with Maltol.[27]

C. albicans budding yeast cells displayed the highest iron content per protein concentration followed by C. albicans hyphae and S. cerevisiae. Maltol treatment of Fe(TOB) endocytosis labeled C. albicans or S.cerevisiae cells restored the iron content to that of untreated cell levels (Figure 3(b)).

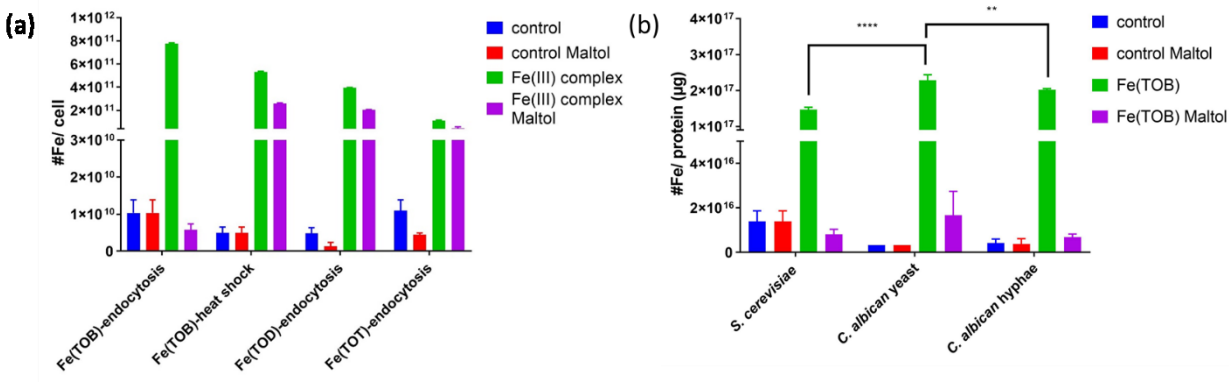


Figure 3. Total Fe content in yeast cells upon (a) Endocytosis and heat treatment with 10 mM Fe(TOB) complexes, Endocytosis labeling with 10 mM Fe(TOD) and Endocytosis labeling with 10 mM Fe(TOT) in S. cerevisiae (b) Endocytosis labeling of 10 mM Fe(TOB) treatment with S. cerevisiae, C. albicans yeast and C. albicans hyphae as measured by ICPMS. Mean ± SE is reported, (****) p < 0.0001 and (**) p < 0.001, n=3.

2.7. Scanning Electron Microscopy (SEM) experiments.

Fe(TOB) labeled S. cerevisiae cells were characterized by using SEM (Figure 4). Inspection of the micrograph suggests that there are drastic changes in the cell surface morphology, which supports interaction of the complex with the cell wall. This result is supported by the fact that the Fe(TOB) complex binds strongly to β-glucan polymer, which is abundantly present in the cell wall.[35] The exact nature of the interaction is not clear, but is facilitated by the open coordination site of the Fe(III) complexes, suggesting that the Fe(III) binds to a component of the β -glucan polymer.

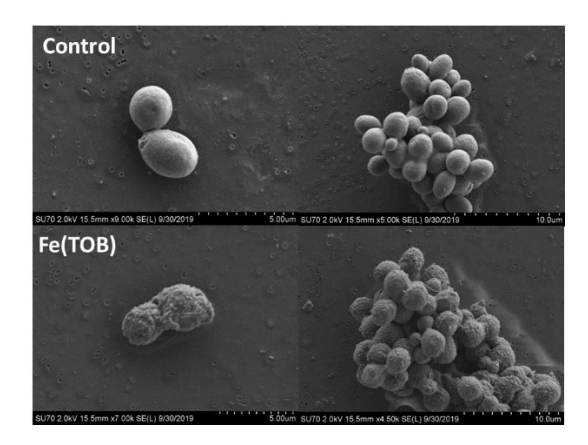


Figure 4. Scanning electron micrograph of control (top) and Fe(TOB) labeled S. cerevisiae.

2.8. Optimizing matrix for T₁ and T₂ water proton relaxation measurements.

It is important to evaluate imaging agents in a matrix to simulate tissue.[36,37] For cell studies, the ideal matrix should mimic the extracellular tissue environment with low background signal. Furthermore, the gel formation should be reproducible and the gel matrix should suspend the cells during the NMR/MRI acquisition experiment window. Other practical factors including moderate gelation time, potential for microbial growth and cost were also taken into account for the selection of the matrix. Based on these criteria, bovine skin collagen, agarose and gelatin were chosen as potential matrices for the proton relaxivity experiments.

Gelatin is hydrolyzed collagen and contains smaller peptides compared to collagen.[38] It is inexpensive and is commonly used as a gelling agent in food and drugs.[39,40] Gelatin was used in concentrations 2-20% (w/v) to prepare gels. The gelation times for gelatin were relatively lengthy and provided enough time to suspend the cells upon reaching room temperature. The background T_2 value did not change significantly with increase in concentration of gelatin (Figure S17). By contrast, gelation of collagen was not as reproducible for suspension of cells.

Agarose gel phantoms have been used extensively in NMR phantom experiments.[41,42] Agarose gelled too quickly and also produced very broad Z-spectra (Figure S18). However, samples suspended in 0.05% (w/v) agarose displayed high background T_2 water proton shortening, reducing the contrast between the Fe(TOB) labeled and control cell samples on 4.7 T animal MRI scanner at 37 °C (Figure S16). Similarly, only small differences in the broadening of Z-spectra were observed for agarose blank, control and Fe(TOB) labeled cells on the 9.4 T NMR spectrometer (Figure S15). Agarose forms a structurally defined matrix with an ordered hydration sphere leading to more efficient spin-spin (T_2) proton relaxation.[43-45]

For futher NMR experiments, the gelatin composition was optimized to 15% (w/v) for suspending yeast cells. The gels polymerized over time leading to sharp water resonances in 1H NMR (Figure S19) and Z-spectra that have less broadening (Figure S18). As a result of polymerization, the difference in the rate constants associated with water proton T_2 processes between the blank and cell experiments was more pronounced. The gelatin gel was able to uniformly suspend the yeast cells for 2.5 h at 37 $^{\circ}$ C. Based on these results, the optimum experimental window was found to be up to 2.5 h after gelation.

Serial dilution assays with *S. cerevisiae* and *C. albicans* on 15% (w/v) gelatin solid plate did not show any significant growth even after 2 days, supporting sterility of the media (Figure S21). The serial dilution spots were inoculated on fresh YEPD media plate and grown for 2 days at 30 °C. The resulting media plate displayed growth of all the serial dilution cells (Figure S22). This observation implies cell proliferation is slow in the absence of media in the 15% (w/v) gelatin matrix during the duration of the NMR experiment.

Fe(TOB) treated and control cells were suspended in 15% (w/v) gelatin. The T₁ water proton shortening was minimal in both phenotypes of Fe(TOB) labeled *C. albicans*. Moreover, there was no statistical difference between control and Fe(TOB) labeled cells in both hyphae and yeast phenotype (Figure S23) when normalized for protein content. Such quenching of T₁ agents in cells is reported in the literature and was attributed to slow water exchange through the cell wall of yeast.[26] Additionally, the hydrophobicity of the cell wall may contribute to lowered water exchange.[27]

The modulation of T_2 water proton relaxation, expressed as a rate constant (R_2), on the other hand, was significantly enhanced in Fe(TOB) labeled samples for both phenotypes (Figure 5). Maltol treatment restored the T_2 proton relaxation, expressed as the R_2 rate constant, to that of the untreated cells for Fe(TOB) labeled cells in both phenotypes.

The detection limit of Fe(TOB) labeling was investigated by mixing the Fe(TOB) labeled cells with control cells in both *C. albicans* yeast and hyphae. The percentage of Fe(TOB) labeled cells was increased while keeping the total protein content of the samples constant at 125 μ g/mL protein (Figure 6). The samples were uniformly suspended in 15% (w/v) gelatin and T₁ and T₂ constants were measured on the samples. As expected, the water proton T₁ constants did not markedly change upon addition of Fe(TOB) labeled cells (Figure S24). The T₂ effect on water protons, on the other hand, increased with an increase of Fe(TOB) labeled cells (Figure 6).

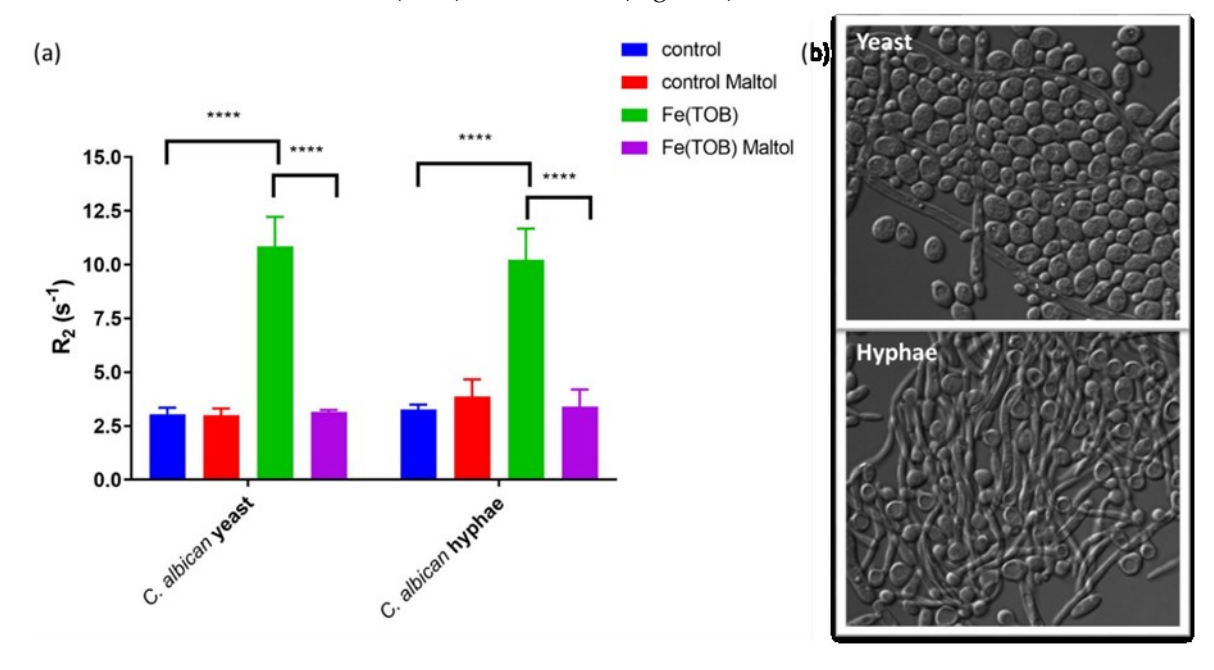


Figure 5. (a) R_2 values of water protons using CPMG sequence on 9.4 T NMR spectrometer with *C. albicans* yeast and hyphae cells suspended in 15% (w/v) gelatin at 37 °C. All cell samples contain ~125 µg protein/mL. Mean \pm SE is reported, (****) p < 0.0001 and n = 3 for cells. (b) Microscopy images of *C. albicans* yeast and hyphae cells.

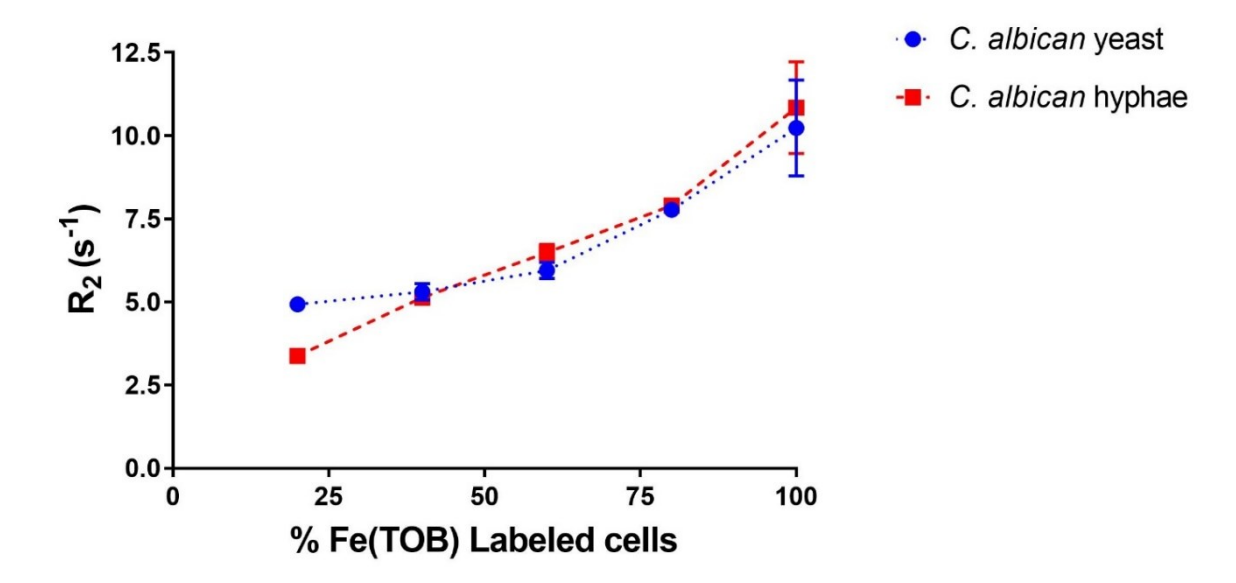


Figure 6. R_2 values of water protons determined using CPMG sequence on samples containing increasing concentration of Fe(TOB) labeled cells suspended in 15% (w/v) gelatin in 9.4 T NMR spectrometer.

2.10. Cell viability

Serial dilution assays were performed on control and Fe(TOB) labeled cells for both *S. cerevisiae* and *C. albicans* (Figure S25-S29). The *S. cerevisiae* and *C. albicans* yeast cells were spotted on YEPD media plate and grown for 2 days at 30 °C. The *C. albicans* hyphae cells were grown in SPIDER media for 2 days at 30 °C and photographed. The effect of Maltol on cell viability of *C. albicans* was also tested by serial dilution assay. Neither treatments of 10 mM Fe(TOB) or 10 mM Fe(TOB) and Maltol have adverse toxicity effects on the cells. The high tolerance of Fe(TOB) complex is promising and bodes well for labeling cells for MRI tracking in animal models.

3. Discussion

Non-invasive probes are needed to monitor in real time the dissemination, progression and potency of antifungal treatments of candidiasis. Considerable effort has been reported towards the development of non-invasive probes to study these infections using luciferase catalyzed bioluminescence and positron induced tomography (PET).[23,46-49] However, the lack of probes for labeling yeast for improved MRI contrast is surprising, especially given the advantages of high resolution and unlimited depth penetration of this modality.

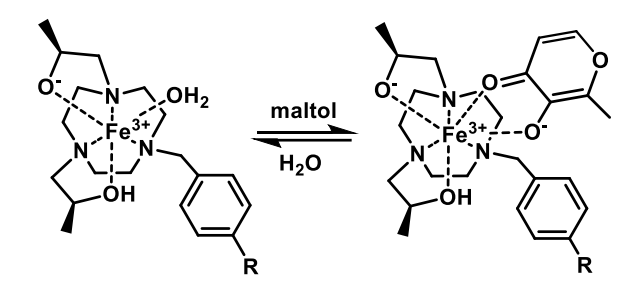
Methods for labeling of yeast with small molecule metal complexes must take into account the yeast cell wall. The cell wall is the outermost organelle of the yeast cells and constitutes 26-32 % of biomass of the yeast cells.[35,50] The cell wall is an accessible target for cellular labeling which does not require the metal complexes to cross the lipid membranes. Moreover, yeast cells have unique β -glucan based cell walls as opposed to peptidoglycan based cell wall in bacteria.[51,52] Selective labeling with β -glucan based cell wall could potentially provide specific labeling and detection of yeast cells over other pathogenic bacterial cells. Our studies here were based on a new class of Fe(III) MRI contrast agent that have a special affinity for the β -glucan containing particles made from the yeast cell wall.[27] We wondered whether the cell wall of live yeast would similarly be labeled with the Fe(III) complexes. Moreover, the change in morphology switching of yeast cells in infectious form may provide a further index of progression. We hypothesized that the change in morphology would affect the magnetic susceptibility of the labeled yeast and produce a unique MRI signature.

Cell association was studied and optimized by using *S. cerevisiae* (Baker's yeast) as a model organism by exploring a series of Fe(III) macrocyclic complexes as paramagnetic agents.

Endocytosis based labeling of *S. cerevisiae* cells with complexes that contain open coordination sites such as Fe(TOBA) and Fe(TASO) lead to broadening of Z-spectra (Figure 1, S4-S5). No such broadening was observed in cells labeled with closed coordination complexes such as Fe(TOT) and Fe(TOTz) (Figure S6-S7). The greater broadening of the Z-spectra corresponds to a larger amount of Fe(III) content in the yeast (Figure S11). Thus, the open coordination site on the Fe(III) center must be critical for interaction with the yeast cells.

Heat shock was also investigated as a means of promoting cell association of complexes into yeast cells. Heat shock treatment of S. *cerevisiae* cells in the presence of Fe(TOB) led to samples with even more pronounced broadening of Z-spectra. The observed broadening of Z-spectra with Fe(III) complexes is unusual in comparison to Gd(III) based T₁ agents that produce narrowed Z-spectra from quenching of magnetization transfer (MT) upon cellular entrapment.[6] The presence of these Gd(III) based T₁ agents leads to perturbations in the MT process leading to a low degree of saturation in the bulk water, thus narrowing the Z-spectra.[53,54]

Both endocytosis and heat shock treatments produced significant cellular association of Fe(TOB) as detected through ICP-MS experiments with no apparent toxicity to the yeast cells (Figure 3(a), Figure S25-S26). Interestingly, endocytosis exhibited the highest Fe cellular association after only 30 min of incubation to give on the order of 10^{10} - 10^{11} Fe/cell in Fe(TOB) labeled *S. cerevisiae*. These values were comparable to the cell association achieved in Gd-HPDO3A labeled mammalian cells and a magnitude lower than a previously reported Fe(III) complex incorporated into yeast cells through electroporation.[4,6,41] Endocytosis was chosen as the preferred mode due to simplicity, ease of scale up and higher levels of incorporation of complex.



R = H, C(O)NHCH₂CH₂NH-dansyl

Scheme 2. Proposed tertiary complex with Maltol and Fe(III) complexes

Interesting differences emerged when the Fe(III) complex labeled *S. cerevisiae* cells were treated with Maltol and the total iron content was measured by using ICP-MS. The cell media for Fe(III) complex labeled cells turned red in color upon Maltol treatment, indicating the release of Fe(III) complex to give the Maltol ternary adduct (Scheme 2). The ternary interaction with Maltol is unique to Fe(TOB) or other open coordination analogs and is not observed in Fe(TOT).[27] Interestingly, Maltol was able to restore the Fe content in the cells to pre Fe(TOB) treatment levels in endocytosis labelled cells, but not in heat shock labeled cells (Figure 3(a)). The inability of Maltol to remove the Fe(III) complex was also observed for Fe(TOD) treated cells.

These results suggest that endocytosis treatment of yeast with Fe(TOB) produces an Fe(III) complex bound to the cell wall, which is released upon Maltol treatment as observed in case of glucan particles (GP). Another possibility is that Fe(TOB) is internalized in the cytoplasm in cells and Fe(TOB)-Maltol complex is able to cross the cellular membrane and cell wall with relative ease. To further investigate the cell wall interaction in endocytosis of Fe(TOB), scanning electron microscopy (SEM) was carried out. The differences in surface morphology between control cells and Fe(TOB) treated cells suggests that Fe(TOB) interacts at the surface of the cells (Figure 4). *C. albicans* samples also displayed complete reversibility of Fe(TOB) labeling when treated with Maltol under similar conditions, suggesting cell wall localization of Fe(TOB). The proposed localization of Fe(TOB) in this case is depicted in the Figure 7(a).

Incomplete retrieval of iron complex by Maltol in heat shocked treated yeast indicates a distinct localization for the Fe(TOB) complex under these conditions. By comparison, heat shock treatment with analogous Co(II) complexes showed a localized punctate pattern suggesting localization by a secretory pathway.[30,31] It is possible that heat shock treatment enhanced the endocytosis mediated cell association resulting in the organeller entrapment of the complex in the secretory pathway. This will pose an additional membrane for the Fe(TOB)-Maltol complex to cross to be released in the cell media resulting in inefficient retrieval of Fe(TOB). We propose that organeller entrapment of Fe(TOD) (Figure 2), also led to inefficient retrieval of iron complex upon Maltol treatment. Interestingly, Maltol was able to release Fe(TOD) labeled from glucan particles (GP).[27] This suggests that crossing an additional membrane due to organeller entrapment diminishes the efficiency of Maltol mediated retrieval of the Fe(III) complex. The proposed localization of Fe(TOB) through heat shock incubation and endocytosis treatment of Fe(TOD) is depicted in Figure 7(b) and Figure 7(c).

(a) Fe(TOB) Endocytosis

(b) Fe(TOB) Heat treatment

(c) Fe(TOD) Endocytosis

Cell wall

Plasma
Membrane

Vacuole

Fe(TOB)

- Fe(TOB)

- Fe(TOD)

Figure 7. Schematic representing the uptake and cell association with tentative localization of Fe(III) complexes. (a) Endocytosis treatment of Fe(TOB) (b) Heat treatment of Fe(TOB) and (c) Endocytosis treatment of Fe(TOD).

Cell wall localization of Fe(TOB) should lead to complex loading that is proportional to the surface area of the cells. It was thus expected, that in samples with equal number of cells, the filamentous *C. albicans* hyphae would show higher Fe(TOB) cell wall incorporation than the ellipsoidal *C. albicans* yeast cells. For *C. albicans*, the yeast phenotype proliferates through budding, resulting in exponential growth in cell numbers. Hyphae, in contrast, exhibit apical growth resulting in longer cells. The total hyphae number however, remains unchanged.[16] Due to this, it is challenging to access cell numbers for hyphae samples for comparison. Instead, total protein content as a measure of biomass was used for normalization.

Surprisingly, *C. albicans* budding yeast phenotype displayed the highest cellular association among the biomass normalized samples of *S. cerevisiae* and *C. albicans* (Figure 3(b)). Assuming the *S. cerevisiae* yeast phenotypes to be spherical in shape with diameters in the range of (5±2) μ m, the estimated cell concentration of Fe(TOB) complexes in cells was calculated to be ~ 19 M for Fe(TOB). Using the biomass normalized volumes reported in the literature and Fe cellular association obtained

in protein normalized samples with ICP-MS measurements, the concentration for Fe(TOB) per cell was found to be \sim 26 M in yeast and \sim 5.5 M in hyphae cells.[16]

Assuming that the cell wall composition to be similar in both yeast and hyphae, this disparity between the Fe(TOB) concentration per cell between *C. albicans* budding yeast and hyphae despite higher cell association of Fe(TOB) in *C. albicans* yeast cells indicates that the complex cellular association is due to the larger number of yeast cells in the sample that have a correspondingly larger surface area. The proclivity of hyphae cells towards forming longer cells instead of increased number of filamentous cells would suggest that a sample containing the same biomass of cells could have a large number of yeast cells compared to filamentous hyphae cells. As a result, the yeast samples could have higher total surface area compared to hyphae cells despite the individual hyphae cells being longer than individual yeast cells.[55] Correlations were obtained in the literature between biomass (dry weight) and surface area of these phenotypes.[16] Under the conditions used in our study the surface area ratio between yeast and hyphae is ~1.2:1 for 1 µg of *C. albicans*.[16,56]

The water proton T₁ and T₂ relaxation times, given as rate constants (R₁ and R₂, respectively) of the Fe(TOB)-labeled yeast cells were investigated in order to determine the best method for monitoring labeled cells. The Z-spectra broadening in the case of Fe(TOB) was attributed to yeast cell loading of paramagnetic metal complex leading to faster T₂ proton relaxation. Liposomes loaded with Gd-based agents under limited water exchange conditions has been shown to display high T₂ proton relaxation due to large contributions from magnetic susceptibility. For liposomal systems, the contribution of paramagnetic complex loading towards the overall R₂ is defined by the following equation.[33,57]

Equation 1

$$R_2^{cell} = R_2^{SUSC} + R_2^{EXCH}$$

Where, R_2^{SUSC} is the contribution from magnetic field inhomogenieties caused by compartmentalization of the paramagnetic liposome and R_2^{EXCH} constitutes the water exchange across the cellular membrane and R_2^{cell} represents that of the cell (or liposome). The susceptibility contribution is dependent on the shape of the labelled vesicle, the effective magnetic moment (μ_{eff}) of the paramagnetic complex and the concentration of the paramagnetic center.[33,57] Heat shock treatment is likely to enhance the complex uptake through a secretory pathway as found in the literature.[31] The Fe(III) complex cell association, though lower than in case of endocytosis, could lead to concentrated compartmentalization of complex into organelles in the secretory pathway to potentially enhance the R_2^{SUSC} contribution and lead to additional broadening in the Z-spectra.

Study of the differences in R_2 between control cells and Fe(TOB) labeled cells was found to be matrix sensitive. Matrices such as agarose, collagen and gelatin were chosen based on biological relevance. 15% gelatin (w/v) was found to provide optimum reproducibility in R_2 at 37 °C. The cells were uniformly suspended in the gel during the NMR experiment and the gel was resistant to microbial growth for 2 days without additives.

Fe(TOB) interacting with the β -glucan based hydrophobic cell wall is likely to modify the second sphere water around the Fe(TOB) complex leading to quenched T₁ effects on proton relaxation.[27] *S. cerevisiae* cells, being ellipsoidal in shape, would likely enhance the magnetic susceptibility contribution to the T₂ based relaxation. Furthermore, the turgidity of cells due to presence of cellular plasma membrane could provide additional organizational structure to the paramagnetic vesicle to further enhance the T₂ based relaxation compared to Fe(TOB) labeled glucan particles (GP). This hypothesis can easily be tested by Fe(TOB) labeling of filamentous (hyphae) *C. albicans*. The filamentous shape of *C. albicans* hyphae could potentially lead to larger magnetic susceptibility contribution further enhancing the T₂ water proton relaxation as long as they have the same localization and loading of Fe(TOB).

The T_2 relaxation times were measured on biomass-normalized samples of C. albicans yeast and hyphae samples labeled with Fe(TOB). As expected from ICP-MS studies, both yeast and hyphae cells displayed similar relaxation rate constants, R_2 . This is most likely the result of larger total

surface area in yeast samples compared to hyphae samples. In addition, *C. albicans* hyphae cells overexpress various adhesive proteins that aids cell adhesion to form fungal biofilms.[58-60] It is possible that the cells could be aggregating on the microscopic level and further reducing the available surface area for Fe(TOB) interaction.

It is noteworthy that despite the lower cellular association of Fe(TOB), the R₂ relaxation rate constants were comparable between the yeast and hyphae samples. This result suggest that there is indeed a higher bulk magnetic contribution in case of hyphae cells resulting in greater water proton T₂ shortening.

4. Materials and Methods

4.1. Instrumentation.

A Varian Inova 500 MHz NMR spectrometer equipped with FTS Systems TC-84 Kinetics Air Jet Temperature Controller was used to collect CEST NMR data and ¹H NMR spectra. Absorbance spectra were collected using a Beckman-Coulter DU 800 UV-vis Spectrophotometer equipped with a Peltier temperature controller. Fluorescence microscopy was done on Zeiss Axioplan2 microscope. The cell viability images were taken using Biorad Chemidoc XRS+ molecular imager. Optical density measurements were done using Dynex Spectra MR plate reader. T¹ and T² relaxation measurements were performed on a 11.7 Tesla NMR spectrometer. Concentration of Fe in yeast cells was determined by using Thermo X-Series 2 inductively coupled plasma mass spectrometry (ICP-MS).

4.2. Materials.

Nitric acid at 65-70% with greater than ≥99.999% purity (trace metals basis) was obtained from BeanTown Chemical. 100 ppm Fe standard solutions were purchased from Inorganic Ventures. Reagent grade Gelatin was purchased from VWR life sciences. Nutrient broth pH 6.9 without NaCl was purchased from Millipore Sigma. D-(-)-Mannitol was purchased from Alfa Aesar. Bovine collagen (3 mg/mL) was obtained from Advanced Biomatrix. For yeast experiments, cultures were grown on standard YEPD [Yeast extract (10g/L), peptone (20g/L) and Dextrose (2%)] liquid or semisolid agar media. For hyphae phenotypes SPIDER media [Nutrient Broth (20g/L), Mannitol (20g/L), K2HPO4(4g/L), pH adjusted to 7.2 with NaOH].

4.3. Cell culture and labeling.

S. cerevisiae of the Sigma1278b strain background was used for the preliminary studies.[28] The specific strain used (PC538) is a typical wild-type (WT) strain with the following genotype: *MATa ste4 FUS1-HIS3 FUS1-lacZ ura3-52*,[29] which was used for experiments in the study. PC538 yeast cells were grown in YEPD [Yeast extract (10g/L), peptone (20g/L), dextrose (2%)] liquid media. Yeast cells were grown to midlog phase. All centrifugations were done at 5000x g. Cells were harvested by centrifugation, and cell pellets were washed with Millipore water. Harvested control cell pellet was suspended in Millipore water and used for experiments. Optical density measurements were done at 600 nm to obtain the cell density to determine the approximate number of cells.

For endocytosis, the cell pellet was treated with 10 mM Fe(III) complexes and incubated at 30 $^{\circ}$ C for 30 min with continuous shaking. The cells were washed and suspended in 1x PBS. Optical density measurements were done at 600 nm to obtain cell numbers.

For heat shock, the resulting cell pellet was treated with 10 mM Fe(TOB) complexes in solution in 50% (v/v) PEG 3350 solution. The cells were incubated at 30 °C for 30 min with continuous shaking. After incubation, the cells were incubated at 42 °C for 10 min. For recovery after heat shock, the cells were then incubated at 30 °C with continuous shaking for 4 h. The cells were washed and suspended in 1x PBS. Optical density measurements were done at 600 nm to obtain the cell density to determine the approximate number of cells.

C. albicans for the study was the strain SC5314, isolated from a patient with systemic candidiasis.[11,61,62] For the growth of the budding yeast form, the cells were grown YEPD liquid

media for 16 h. Cells were harvested by centrifugation, and cell pellets were washed with Millipore water. For endocytosis, the cell pellet was treated with 10 mM Fe(TOB) and incubated at 30 $^{\circ}$ C for 30 min with continuous shaking. The cells were washed and suspended in 1x PBS. Optical density measurements were done at 600 nm to obtain cell numbers.

For growing the hyphae of *C. albicans*, cells were grown in YEPD liquid media for 16 h, harvested by centrifugation and optical density measurement were done at 600 nm. The optical density being ~33 OD was diluted to 10 OD. The cells were washed thrice with 1x PBS. The cells were harvested by centrifugation and were diluted to 0.2 OD and grown for 4 h at 37 °C with continuous shaking in Spider media.[63] Post incubation cells were harvested by centrifugation, and cell pellets were washed with Millipore water. For endocytosis, the cell pellet was treated with 10 mM Fe(TOB) and incubated at 30 °C for 30 min with continuous shaking. The cells were washed and suspended in 1x PBS. Optical density measurements were done at 600 nm to obtain cell numbers.

4.4. Fluorescence Microscopy.

C. albicans (budding yeast and hyphae) cells were collected and suspended in 1x PBS. The cells were heat killed at 60 °C for 15 min before preparing the glass slides for imaging by fluorescence microscopy. Fluorescence imaging was done using phase contrast channel on a Zeiss Axioplan2 fluorescence microscope.

For confocal microscopy on *S. cerevisiae* yeast cells were washed three times in water before preparing the samples for imaging. The samples were added under an synthetic dextrose (SD) agar pad to avoid sample dehydration during the experiment.[64]

4.5. Pierce Protein assay.

The cells were cultured in triplicate and were collected by centrifugation. The resulting cell pellets were stored at -80 °C for 16 h. The cells were thawed to room temperature and proteins were extracted by the addition of trichloracetic acid (TCA) buffer containing 10% TCA; 10 mM Tris-HCl pH 8; 25 mM ammonium acetate, and 1 mM EDTA. Acid-washed glass beads were added to the scaffold and cell pellet mixture. Cells were lysed by three consecutive 90 sec vortex pulses with 1 min rests on ice using fast prep multi-vortex (Labline instrument, Melrose, IL). Proteins were precipitated by centrifugation at 4 °C at 16000 g for 10 min. Protein pellets were thoroughly re-suspended using resuspension buffer containing 0.1 M Tris-HCl pH 11 and 3% SDS by boiling the suspension for 5 min at 95 °C. Total protein concentration was measured using Biorad BCA protein assay kit (Pierce™ Microplate BCA Protein Assay Kit catalog # 23252). The total protein content was plotted against the optical density at 600 nm (OD600) for the cells. The data was fit to a linear regression graph in graphpad prism.

4.6. Z-spectra measurements on Fe(III) complex labeled yeast.

All samples were suspended in 1x PBS for analysis. Z-spectra have been acquired in a range of \pm 100ppm by acquiring a total of 201 data points (steps of 1 ppm) with B₁ = 3, 6, 12 μ T at 37 °C.

4.7. Maltol removal of Fe(TOB) labeled yeast.

To the Fe(TOB) labeled yeast, 10 mM Maltol solution was added. The particles were incubated for 3 h at 30 $^{\circ}$ C. After incubation, the particles were harvested through centrifugation followed by 3 times 1x PBS wash. Both supernatant and pellet were saved for ICP-MS analysis.

4.8. Matrix preparation.

Bovine collagen, agarose and gelatin were used to study the effect of gelling agent on the matrix relaxation times. Samples with 2.4 mg/mL collagen were prepared using the protocol reported in literature.[26] Concentration of gelling agents were varied between 1%-25% (w/v) for gelatin and 0.5-4% (w/v) agarose. A series of test matrices were prepared by mixing the agents with distilled water at room temperature. The resulting samples were heated to dissolve the solid particles with constant

526

527

528

529

530

531

532

533

534

535

536

537

538

539

540

541

542

543

544

545

546

547

548

549

550

551

552

553

554

555

556

557

558

559

560

561

562

563

564

565

566

567

568

stirring. The resulting gels were further tested to investigate the gelation times, cell suspension threshold and experimental window for the cell phantom experiments.

Culture plates were prepared with the various matrices and nutrient supplementation to examine the susceptibility of yeast growth during the experiments. Culture plates with only gelation matrix was prepared to examine the sterility of the matrix.

4.9. T₁ and T₂ water proton relaxation measurements of yeast cells and data analysis.

Cells were washed three times with 1x PBS. The cells were normalized with respect to the total protein content (~125 µg/ml) and suspended in 15% (w/v) gelatin gel using the referenced protocol[65] in 5 mm borosilicate NMR sample tubes. The relaxation rates of the cells were measured on a 9.7 T NMR spectrometer at 37 °C using Inversion recovery for T₁ and Carr-Purcell-Meiboom-Gill (CPMG) spin echo for T₂ protocol.[66] Briefly, T₁ relaxation times of serial dilutions were measured using an inversion-recovery with the following parameters: relaxation delay = 20 s, echo time array starting from 0.5-5 s, receiver bandwidth = 28 ms. T₂ relaxation times were measured using Carr-Purcell-Meiboom-Gill (CPMG) sequence with a fixed TR of 10 s and TE times ranging from 100-3000 ms in 100 ms increments. The relaxation rate of each sample calculated using non-linear regression analysis in graphpad prism. Alternatively, T₁/T₂ relaxation times were determined on a 4.7 Tesla MRI system as reported previously.[26] Briefly, T1 relaxation times of serial dilutions were measured using an inversion-recovery, balanced steady-state free precession (bSSFP) acquisition with the following parameters: TE/TR=1.5/3.0 ms, flip angle=30°, inv. repetition time=10 s, segments=8, frames=100. T2 relaxation times were measured using a multi-echo, Carr-Purcell-Meiboom-Gill (CPMG) sequence with a fixed TR of 4200 ms and TE times ranging from 20-1200 ms in 20 ms increments. The relaxation rate of each sample was calculated using non-linear regression analysis within MATLAB (MathWorks, Natick MA) and relaxivities were then calculated by linear regression (concentration vs. relaxation rate).

4.10. Scanning Electron Microscopy (SEM) on glucan particles.

The samples were prepared by a method previously reported in literature.[27,67] Briefly, control and Fe(TOB)treated cells were concentrated by syringe filtration by a 0.2 micron Whatman nucleopore polycarbonate filter paper with 1 mL syringe (GE Whatman, catalog #889-78084, Maidstone, UK). Cells were rinsed with buffer by syringe, treated with 100 % ethanol by syringe and incubated for 15 min. The filter paper was removed from the holder, placed in a petri dish and treated with hydroxymethyldiazane (HMDS). Samples were placed at 4 °C for 16 h and imaged the following day.

4.11. Cell viability assay.

Aliquots of control cells and complex treated cells were washed two times with 1x PBS. Serial dilution assays were performed by spotting 10 μ L of serial 10-fold dilutions of the cultures with optical density OD600 of 0.8 on YEPD semi-solid agar media for *S. cerevisiae* and *C. albicans* yeast and Spider semi-solid media for *C. albicans* hyphae cultures. The plates were incubated and photographed after 24 h for *C. albicans* and 48 h for *S. cerevisiae*.

4.12. Determination of iron in the yeast cells.

The amount of Fe in the yeast cells was determined by using inductively coupled plasma mass spectrometry (ICP-MS) (Thermo X-Series 2). After the internalization experiments, the yeast cells with and without Fe(III) complex were collected in 200 μ L milli-Q (Millipore) water. Yeast cell solutions (100 μ L) were digested with metal free nitric acid (900 μ L) (65-70%). After three-day digestion process, the samples were diluted to 2% HNO₃, 30 ppb cobalt standard solution in 10 mL milli-Q (Millipore) water and analyzed by ICP-MS. As the internal standards, cobalt and indium standard solutions were used.

569 4.13. Statistical analysis.

Results were expressed as mean value \pm standard error (SE). Statistical analyses were performed using one-way ANOVA analysis followed by Tukey's multiple comparisons test by using Graphpad Prism 8. A P value of less than 0.05 was regarded as significant for cellular association and viability studies, P value of less than 0.5 was regarded as significant for T_1 measurements on cells.

573574

575

576

577

578

579

580

581

582

583

584

585

586

587

588

589

570

571

572

5. Conclusions

This study demonstrates that paramagnetic Fe(III) based MRI probes can be used to label pathogenic *C. albicans* as well as the domesticated *S. cerevisiae*. Endocytosis was the most efficient method for cellular labeling with Fe(TOB); studies supported cell wall localization of Fe(TOB) in both *S. cerevisiae* and *C. albicans* when this method was used. The Fe(TOB) labeled cells displayed strong enhancement in water proton T₂ relaxation which may be useful for tracking the yeast *in vivo*. The strongly enhanced T₂ over T₁ relaxation times of Fe(TOB) associated with yeast would allow *in vivo* discrimination of Fe(TOB) labeled yeast over free complex.

Fe(TOB) labeled yeast cells may find application for the study of invasive candidiasis in animals. We envision that yeast cells labeled with paramagnetic probes would be injected into animals to study the progression of the yeast infection in the host. Alternatively, given that several of the Fe(III) macrocyclic complexes studied here produce MRI contrast in mice, studies are warranted to determine whether yeast infections might be detected by administration of the Fe(III) MRI contrast agents into the animal. The success of this type of study would rely on tuning the biodistribution of the contrast agent to target the site of infection.[24,25]

- 590 Supplementary Materials: The following are available online at www.mdpi.com/xxx/s1, Figure S1: title, Table S1: title, Video S1: title.
- 592 **Author Contributions:** Conceptualization, J.R.M., A.P., P.J.C.; methodology, A.P., D.A, E.M.S, P.J.C and J.A.S; resources, J.R.M., P.J.C and J.A.S.; writing—original draft preparation, A.P. and J.R.M.; writing—review and editing, J.R.M., A.P., D.A. and P.J.C.; supervision, J.R.M.; project administration, J.R.M. and P.J.C.; funding acquisition, J.R.M. and P.J.C. All authors have read and agreed to the published version of the manuscript.
- Funding: JRM thanks the NSF (CHE-1710224) for support of this work. P.J.C is supported by a grant from the NIH (GM#098629). The authors would also like to thank Chemistry Instrument Center (CIC), University at Buffalo. This work utilized ICP-MS that was purchased with funding from a NSF Major Research Instrumentation Program (NSF CHE-0959565) and National Institutes of Health (S10 RR029517). The confocal imaging studies were funded by National Science Foundation Major Research Foundation grant # DBI 0923133.
- Acknowledgments: The authors would like to thank Prof. Laura Rusche for providing SC5314 *C. albicans* strain for the studies. We thank Peter Bush for providing assistance with electron microscopy. We thank Gail Willsky for suggestions on the manuscript.
- Conflicts of Interest: JRM is a co-founder of Ferric Contrast, Inc., a company with a focus on iron MRI contrast agents. The funders had no role in the design of the study; in the collection, analyses, or interpretation of data; in the writing of the manuscript, or in the decision to publish the results.

References

607

- Branski, L.K.; Gauglitz, G.G.; Herndon, D.N.; Jeschke, M.G. A review of gene and stem cell therapy in cutaneous wound healing. *Burns* **2009**, *35*, 171-180, doi:https://doi.org/10.1016/j.burns.2008.03.009.
- Nicholls, F.J.; Ling, W.; Ferrauto, G.; Aime, S.; Modo, M. Simultaneous MR imaging for tissue engineering in a rat model of stroke. *Sci. Rep.* **2015**, *5*, 14597, doi:10.1038/srep14597.
- June, C.H.; O'Connor, R.S.; Kawalekar, O.U.; Ghassemi, S.; Milone, M.C. CAR T cell immunotherapy for human cancer. *Science* **2018**, *359*, 1361-1365, doi:10.1126/science.aar6711.
- Ferrauto, G.; Di Gregorio, E.; Dastrù, W.; Lanzardo, S.; Aime, S. Gd-loaded-RBCs for the assessment of tumor vascular volume by contrast-enhanced-MRI. *Biomaterials* **2015**, *58*, 82-92, doi:https://doi.org/10.1016/j.biomaterials.2015.04.026.

- 5. Ferrauto, G.; Delli Castelli, D.; Di Gregorio, E.; Langereis, S.; Burdinski, D.; Grüll, H.; Terreno, E.; Aime,
- S. Lanthanide-Loaded Erythrocytes As Highly Sensitive Chemical Exchange Saturation Transfer MRI
- 619 Contrast Agents. J. Amer. Chem. Soc. 2014, 136, 638-641, doi:10.1021/ja411793u.
- 620 6. Delli Castelli, D.; Ferrauto, G.; Di Gregorio, E.; Terreno, E.; Aime, S. Sensitive MRI detection of
- internalized T1 contrast agents using magnetization transfer contrast. NMR Biomed. 2015, 28, 1663-1670,
- 622 doi:10.1002/nbm.3423.
- 623 7. Mota, F.; Ordonez, A.A.; Firth, G.; Ruiz-Bedoya, C.A.; Ma, M.T.; Jain, S.K. Radiotracer Development for
- Bacterial Imaging. *J. Med. Chem.* **2020**, *63*, 1964-1977, doi:10.1021/acs.jmedchem.9b01623.
- Locke, L.; Shankaran, K.; Gong, L.; Stoodley, P.; Vozar, S.L.; Cole, S.L.; Tweedle, M.F.; Wozniak, D.J.
- $626 \hspace{1.5cm} \hbox{Evaluation of peptide-based probes towards in vivo diagnostic imaging of bacterial biofilm-associated} \\$
- 627 infections. ACS Infect. Diseases 2020, 10.1021/acsinfecdis.0c00125, doi:10.1021/acsinfecdis.0c00125.
- 628 9. Kullberg, B.J.; Arendrup, M.C. Invasive Candidiasis. *N. E. J. Med.* **2015**, *373*, 1445-1456, doi:10.1056/NEJMra1315399.
- 630 10. Pfaller, M.A.; Diekema, D.J. Epidemiology of Invasive Candidiasis: a Persistent Public Health Problem.
- 631 Clin. Microbiol. Rev. 2007, 20, 133-163, doi:10.1128/cmr.00029-06.
- Vediyappan, G.; Dumontet, V.; Pelissier, F.; d'Enfert, C. Gymnemic Acids Inhibit Hyphal Growth and
- Virulence in Candida albicans. *PLOS one* **2013**, *8*, e74189, doi:10.1371/journal.pone.0074189.
- Kato, H.; Yoshimura, Y.; Suido, Y.; Shimizu, H.; Ide, K.; Sugiyama, Y.; Matsuno, K.; Nakajima, H.
- Mortality and risk factor analysis for Candida blood stream infection: A multicenter study.
- 636 *J. Infec. Chemotherapy* **2019**, 25, 341-345, doi:10.1016/j.jiac.2019.01.002.
- Arendrup, M.C.; Andersen, J.S.; Holten, M.K.; Krarup, K.B.; Reiter, N.; Schierbeck, J.; Helleberg, M.
- Diagnostic Performance of T2Candida Among ICU Patients With Risk Factors for Invasive Candidiasis.
- 639 Open Forum Infec. Diseases 2019, 6, doi:10.1093/ofid/ofz136.
- Pappas, P.G.; Walsh, T.J.; Zaoutis, T.E.; Sobel, J.D.; Kauffman, C.A.; Andes, D.R.; Clancy, C.J.; Marr,
- K.A.; Ostrosky-Zeichner, L.; Reboli, A.C., et al. Clinical Practice Guideline for the Management of
- Candidiasis: 2016 Update by the Infectious Diseases Society of America. Clin. Infec. Diseases 2015, 62,
- 643 e1-e50, doi:10.1093/cid/civ933.
- 644 15. Saraswat, D.; Kumar, R.; Pande, T.; Edgerton, M.; Cullen, P.J. Signalling mucin Msb2 Regulates
- adaptation to thermal stress in Candida albicans. Mol. Microbiol. 2016, 100, 425-441,
- 646 doi:10.1111/mmi.13326.
- 647 16. Hosseinzadeh, A.; Urban, C.F. Novel insight into neutrophil immune responses by dry mass
- determination of Candida albicans morphotypes. PLOS one 2013, 8, e77993-e77993,
- doi:10.1371/journal.pone.0077993.
- 650 17. Berman, J.; Sudbery, P.E. Candida Albicans: a molecular revolution built on lessons from budding
- 651 yeast. Nat. rev. Genet. 2002, 3, 918-930, doi:10.1038/nrg948.
- Noble, S.M.; French, S.; Kohn, L.A.; Chen, V.; Johnson, A.D. Systematic screens of a Candida albicans
- homozygous deletion library decouple morphogenetic switching and pathogenicity. *Nat. Genet.* **2010**,
- 42, 590, doi:10.1038/ng.60, https://www.nature.com/articles/ng.605#supplementary-information.
- Orlowski, H.L.P.; McWilliams, S.; Mellnick, V.M.; Bhalla, S.; Lubner, M.G.; Pickhardt, P.J.; Menias, C.O.
- Imaging Spectrum of Invasive Fungal and Fungal-like Infections. RadioGraph. 2017, 37, 1119-1134,
- doi:10.1148/rg.2017160110.

- Shih, R.Y.; Koeller, K.K. Bacterial, Fungal, and Parasitic Infections of the Central Nervous System:
- Radiologic-Pathologic Correlation and Historical Perspectives: From the Radiologic Pathology Archives. *RadioGraph.* **2015**, *35*, 1141-1169, doi:10.1148/rg.2015140317.
- Sánchez-Portocarrero, J.; Pérez-Cecilia, E.; Corral, O.; Romero-Vivas, J.; Picazo, J.J. The central nervous
- system and infection by Candida species. *Diagn. Microbiol. Infect. Dis.* **2000**, 37, 169-179, doi:10.1016/s0732-8893(00)00140-1.
- Zhang, P.; Lian, L.; Wang, F. Magnetic resonance imaging features of gelatinous pseudocysts in cryptococcal meningoencephalitis. *Acta Neurologica Belgica* **2019**, *119*, 265-267, doi:10.1007/s13760-018-1033-6.
- Jacobsen, I.D.; Lüttich, A.; Kurzai, O.; Hube, B.; Brock, M. In vivo imaging of disseminated murine
 Candida albicans infection reveals unexpected host sites of fungal persistence during antifungal
 therapy. *J. Antimicrob. Chemother.* **2014**, *69*, 2785-2796, doi:10.1093/jac/dku198.
- Didar Asik, R.S., Samira M. Abozeid, Travis B. Mitchell, Steven G. Turowski, Joseph A. Spernyak and
 Janet R. Morrow. Modulating the Properties of Fe(III) Macrocyclic MRI Contrast Agents by Appending
 Sulfonate or Hydroxyl Groups. *Molecules* 2020, 25, 2291.
- Snyder, E.M.; Asik, D.; Abozeid, S.M.; Burgio, A.; Bateman, G.; Turowski, S.G.; Spernyak, J.A.; Morrow,
 J.R. A Class of FeIII Macrocyclic Complexes with Alcohol Donor Groups as Effective T1 MRI Contrast
 Agents. Angew. Chem. 2020, 132, 2435-2440, doi:10.1002/ange.201912273.
- Patel, A.; Asik, D.; Spernyak, J.A.; Cullen, P.J.; Morrow, J.R. MRI and fluorescence studies of Saccharomyces cerevisiae loaded with a bimodal Fe(III) T1 contrast agent. *J. Inorg. Biochem.* **2019**, 201, 110832, doi:https://doi.org/10.1016/j.jinorgbio.2019.110832.
- Patel, A.; Asik, D.; Snyder, E.M.; Dilillo, A.E.; Cullen, P.J.; Morrow, J.R. Binding and Release of FeIII Complexes from Glucan Particles for the Delivery of T1 MRI Contrast Agents. *ChemMedChem* **2020**, *15*, 1050-1057, doi:10.1002/cmdc.202000003.
- Gimeno, C.J.L., P. O.; Styles, C. A.; Fink, G. R., Unipolar cell divisions in the yeast S. cerevisiae lead to filamentous growth: regulation by starvation and RAS. *Cell* **1992**, *68*, 1077-1090.
- 684 29. Cullen, P.J.; Sabbagh, W., Jr.; Graham, E.; Irick, M.M.; van Olden, E.K.; Neal, C.; Delrow, J.; Bardwell,
 685 L.; Sprague, G.F., Jr. A signaling mucin at the head of the Cdc42- and MAPK-dependent filamentous
 686 growth pathway in yeast. *Genes. Dev.* 2004, 18, 1695-1708.
- 687 30. Patel, A.; Mohammed, A. S.; Cullen, P.J.; Morrow, J.R. Manuscript in preparation.
- Kawai, S.; Hashimoto, W.; Murata, K. Transformation of Saccharomyces cerevisiae and other fungi. *Bioengin. Bugs* **2010**, *1*, 395-403, doi:10.4161/bbug.1.6.13257.
- Samira M. Abozeid, D.A., Janet R. Morrow. Liposomal Fe(III) complexes as T1, T2 and lipoCEST agents.

 Manuscript in preparation.
- Mulas, G.; Ferrauto, G.; Dastrù, W.; Anedda, R.; Aime, S.; Terreno, E. Insights on the relaxation of liposomes encapsulating paramagnetic Ln-based complexes. *Magn. Reson. Med.* **2015**, 74, 468-473, doi:10.1002/mrm.25412.
- Smith, P.K.; Krohn, R.I.; Hermanson, G.T.; Mallia, A.K.; Gartner, F.H.; Provenzano, M.D.; Fujimoto, E.K.; Goeke, N.M.; Olson, B.J.; Klenk, D.C. Measurement of protein using bicinchoninic acid. *Anal. Biochem.* 1985, 150, 76-85, doi:10.1016/0003-2697(85)90442-7.
- 698 35. Nguyen, T.H.; Fleet, G.H.; Rogers, P.L. Composition of the cell walls of several yeast species. *Appl. Microbiol. Biotechnol.* **1998**, *50*, 206-212, doi:10.1007/s002530051278.

- 700 36. Mitchell, M.D.; Kundel, H.L.; Axel, L.; Joseph, P.M. Agarose as a tissue equivalent phantom material for NMR imaging. *Magn. Reson. Imag.* **1986**, *4*, 263-266, doi:10.1016/0730-725x(86)91068-4.
- 702 37. Alexandra Hellerbach , V.S., Andreas Jansen, Jens Sommer. MRI Phantoms Are There Alternatives to Agar? *PLOS one* **2013**, *8*, e70343, doi:doi.org/10.1371/journal.pone.0070343.
- Young, S.; Wong, M.; Tabata, Y.; Mikos, A.G. Gelatin as a delivery vehicle for the controlled release of bioactive molecules. *J. Control Release* **2005**, *109*, 256-274, doi:10.1016/j.jconrel.2005.09.023.
- 706 39. Komaiko, J.; McClements, D.J. Food-grade nanoemulsion filled hydrogels formed by spontaneous emulsification and gelation: Optical properties, rheology, and stability. *Food Hydrocolloids* **2015**, 46, 67-708 75, doi:https://doi.org/10.1016/j.foodhyd.2014.12.031.
- 709 40. Dowling, M.B.; Lee, J.-H.; Raghavan, S.R. pH-Responsive Jello: Gelatin Gels Containing Fatty Acid Vesicles. *Langmuir* **2009**, 25, 8519-8525, doi:10.1021/la804159g.
- Ferrauto, G.; Di Gregorio, E.; Delli Castelli, D.; Aime, S. CEST-MRI studies of cells loaded with lanthanide shift reagents. *Magn. Reson. Med.* **2018**, *80*, 1626-1637, doi:10.1002/mrm.27157.
- 713 42. Dorazio, S.J.; Olatunde, A.O.; Spernyak, J.A.; Morrow, J.R. CoCEST: cobalt(II) amide-appended paraCEST MRI contrast agents. *Chem. Commun.* **2013**, 49, 10025.
- Maaloum, M.; Pernodet, N.; Tinland, B. Agarose gel structure using atomic force microscopy: Gel concentration and ionic strength effects. *ELECTROPHORESIS* **1998**, 19, 1606-1610, doi:10.1002/elps.1150191015.
- 718 44. Stellwagen, J.; Stellwagen, N.C. Internal Structure of the Agarose Gel Matrix. *J. Phy. Chem.* **1995**, *99*, 719 4247-4251, doi:10.1021/j100012a054.
- Griess, G.A.; Guiseley, K.B.; Serwer, P. The relationship of agarose gel structure to the sieving of spheres during agarose gel electrophoresis. *Biophy. J.* **1993**, *65*, 138-148, doi:10.1016/S0006-3495(93)81072-5.
- Hutchens, M.; Luker, G.D. Applications of bioluminescence imaging to the study of infectious diseases.
 Cell Microbiol. 2007, 9, 2315-2322, doi:10.1111/j.1462-5822.2007.00995.x.
- 724 47. Andreu, N.; Zelmer, A.; Wiles, S. Noninvasive biophotonic imaging for studies of infectious disease. 725 *FEMS Microbiol. Rev.* **2011**, *35*, 360-394, doi:10.1111/j.1574-6976.2010.00252.x.
- Morad, H.O.J.; Wild, A.-M.; Wiehr, S.; Davies, G.; Maurer, A.; Pichler, B.J.; Thornton, C.R. Pre-clinical Imaging of Invasive Candidiasis Using ImmunoPET/MR. Front. Microbiol. 2018, 9, doi:10.3389/fmicb.2018.01996.
- 729 49. Bleeker-Rovers, C.P.; Warris, A.; Drenth, J.P.H.; Corstens, F.H.M.; Oyen, W.J.G.; Kullberg, B.-J.
 730 Diagnosis of Candida lung abscesses by 18F-fluorodeoxyglucose positron emission tomography. *Clin.*731 *Microbiol. Infect.* 2005, 11, 493-495, doi:10.1111/j.1469-0691.2005.01155.x.
- 50. Lesage, G.; Bussey, H. Cell wall assembly in Saccharomyces cerevisiae. *Microbiol. Mol. Biol. Rev.* **2006**, 70, 317-343, doi:10.1128/mmbr.00038-05.
- 734 51. Dörr, T.; Moynihan, P.J.; Mayer, C. Editorial: Bacterial Cell Wall Structure and Dynamics. *Front.*735 *Microbiol.* **2019**, *10*, doi:10.3389/fmicb.2019.02051.
- 736 52. Romaniuk, J.A.H.; Cegelski, L. Bacterial cell wall composition and the influence of antibiotics by cell-737 wall and whole-cell NMR. *Philos. Trans. Roy. Soc. B: Biol. Sci.* **2015**, 370, 20150024, 738 doi:doi:10.1098/rstb.2015.0024.
- Tee, Y.K.; Donahue, M.J.; Harston, G.W.J.; Payne, S.J.; Chappell, M.A. Quantification of amide proton transfer effect pre- and post-gadolinium contrast agent administration. *J. Magn. Reson. Imag.* **2014**, 40, 832-838, doi:10.1002/jmri.24441.

- Kurki, T.J.; Niemi, P.T.; Lundbom, N. Gadolinium-enhanced magnetization transfer contrast imaging of intracranial tumors. *J. Magn. Reson. Imag.* **1992**, *2*, 401-406, doi:10.1002/jmri.1880020408.
- Mukaremera, L.; Lee, K.K.; Mora-Montes, H.M.; Gow, N.A.R. Candida albicans Yeast, Pseudohyphal, and Hyphal Morphogenesis Differentially Affects Immune Recognition. *Front. Immunol.* **2017**, *8*, doi:10.3389/fimmu.2017.00629.
- 747 56. Creger, P.E.; Blankenship, J.R. Analysis of gene expression in filamentous cells of Candida albicans 748 grown on agar plates. *J. Biol. Meth.* **2018**, 10.14440/jbm.2018.211
- 749 57. Terreno, E.; Geninatti Crich, S.; Belfiore, S.; Biancone, L.; Cabella, C.; Esposito, G.; Manazza, A.D.; Aime, S. Effect of the intracellular localization of a Gd-based imaging probe on the relaxation enhancement of water protons. *Magn. Reson. Med.* **2006**, *55*, 491-497, doi:10.1002/mrm.20793.
- Li, F.; Svarovsky, M.J.; Karlsson, A.J.; Wagner, J.P.; Marchillo, K.; Oshel, P.; Andes, D.; Palecek, S.P.
 Eap1p, an adhesin that mediates Candida albicans biofilm formation in vitro and in vivo. *Eukaryot. cell*2007, 6, 931-939, doi:10.1128/EC.00049-07.
- The Total Times Technology Times Times Technology Times Technology Times Tim
- 757 60. McCall, A.D.; Pathirana, R.U.; Prabhakar, A.; Cullen, P.J.; Edgerton, M. Candida albicans biofilm development is governed by cooperative attachment and adhesion maintenance proteins. *N.P.J. Biofilms*759 *Microbiomes* **2019**, *5*, 21, doi:10.1038/s41522-019-0094-5.
- Rupert, C.B.; Heltzel, J.M.H.; Taylor, D.J.; Rusche, L.N. Sporadic Gene Loss After Duplication Is
 Associated with Functional Divergence of Sirtuin Deacetylases Among *Candida* Yeast Species. *G3*:

 Genes, Genomes, Genetics **2016**, 6, 3297-3305, doi:10.1534/g3.116.033845.
- Gillum, A.M.; Tsay, E.Y.; Kirsch, D.R. Isolation of the Candida albicans gene for orotidine-5'-phosphate decarboxylase by complementation of S. cerevisiae ura3 and E. coli pyrF mutations. *Mol. Gen. Genet.*1984, 198, 179-182, doi:10.1007/bf00328721.
- Liu, H.; Kohler, J.; Fink, G. Suppression of hyphal formation in Candida albicans by mutation of a STE12
 homolog. *Science* 1994, 266, 1723-1726, doi:10.1126/science.7992058.
- Daniel R. Rines, D.T., Jonas F. Dorn, Paul Goodwin, and Peter K. Sorger. Live Cell Imaging of Yeast.

 Cold Spring Harb. Protoc. 2011, 9, 1026-1041, doi:10.1101/pdb.top065482.
- 770 65. Y, F. Protocol for cell-seeded collagen gels. Availabe online: (accessed on
- 771 66. P. McIntosh, L. CPMG. In *Encyclopedia of Biophysics*, Roberts, G.C.K., Ed. Springer Berlin Heidelberg: Berlin, Heidelberg, 2013; 10.1007/978-3-642-16712-6_320pp. 386-386.
- 773 67. Chow, J.N., Marysa; Prabhakar, Aditi; Free, Stephen J.; Cullen, Paul J. . Impact of Fungal MAPK Pathway Targets on the Cell Wall. *J. Fungi* **2018**, *4*, 93.

775 1.



© 2020 by the authors. Submitted for possible open access publication under the terms and conditions of the Creative Commons Attribution (CC BY) license (http://creativecommons.org/licenses/by/4.0/).